SUPERCONDUCTING CAVITY RESONATORS

A key component of the modern particle accelerator (59) is the device that imparts energy to the charged particles. This is an electromagnetic radio frequency (RF) cavity resonating at microwave frequencies typically between 50 MHz and 3000 MHz. Traditionally, accelerating devices are normal conducting cavities typically made from copper (59). One of the main incentives for using superconducting cavities is that the dissipation in the walls of the copper structure can be substantially reduced. This is especially beneficial for accelerators that operate in a continuous wave (CW) mode or at a high duty factor (e.g., > 1 percent). Superconducting cavities economically provide high CW operating fields. Another benefit is that superconducting cavities can be designed to have a large beam aperture which reduces the beam cavity interactions, allowing higher beam quality and higher beam current.

There are two distinct types of superconducting cavities, depending on the velocity of the particles. The first category is for accelerating charged particles that move at nearly the speed of light, such as electrons in a high-energy linear accelerator [e.g., at TJNAF (1) at Jefferson Lab in Newport News, VA] or a storage ring [e.g., LEP (2) at CERN in Switzerland]. The second type is for particles that move at a small fraction (e.g., 0.01 to 0.3) of the speed of light, such as the heavy ions emerging from a dc high-voltage Van de Graaff accelerator. ATLAS (3) at Argonne National Lab, Argonne, IL is the longest-running heavy ion accelerator facility. Figure 1(a) is a sketch of the typical superconducting accelerating structure of the first type, and Fig. 2(a) is a corresponding photograph (4). There are five accelerating cells that resonate in the TM_{010} mode of the cylindrical cavity. As the particle traverses each half-wavelength ($\lambda/2$) accelerating gap in half a radio-frequency (RF) period, it sees a longitudinal electric field pointing in the same direction for continuous acceleration. Figure 1(b) is a sketch for a structure for low velocity particles, and Fig. 2(b) is a corresponding photograph (5). A coaxial transmission line a quarter wavelength long resonates in the TEM mode. A drift tube is suspended from the end of the hollow center conductor. The structure has two accelerating cells between the ends of the drift tube and the beam hole openings located in the outer conductor of the coax. The accelerating gap is $\beta\lambda/2$, where $\beta = v/c$. Since β is small, λ must be chosen to be large, to achieve a useful acceleration. Therefore a low resonant frequency is chosen, typically 100 MHz. The wavelength also sets the height of the quarter-wave resonator. The example of Fig. 2 has a manageable height of less than one meter.

Large-scale application of superconducting cavities to electron and ion accelerators is now established at many laboratories around the world (6). These accelerators provide high-energy electron and positron beams for elementary particle research, medium-energy electron beams for nuclear physics research, low-energy, heavy ion beams for nuclear research, and high-quality electron beams for free electron lasers. Altogether more than 500 meters of superconducting cavities have been installed worldwide and successfully operated at accelerating fields up to 6 MV/m to provide a total of more than 2.5 GV for a variety of accelerators.

The two most salient characteristics of an accelerating cavity are its average accelerating field, E_{acc}, and the quality factor Q_0. The typical accelerating field at which $\beta \approx 1$ superconducting cavities are now operated routinely is $E_{acc} = 5$ MV/m, and the typical Q_0 value is 2×10^9. The corresponding numbers for low-velocity structures are 3 MV/m and 10^9. Accelerating fields as high as 40 MV/m and Q_0 values as high as 10^{11} have been reached in high-performance $\beta \approx 1$ superconducting test cavities.

The strongest incentive to use superconducting cavities is in accelerators that operate in a continuous-wave (CW) mode, or at a high duty factor (>1%). For CW operation, the power dissipation in the walls of a structure built from normal conducting material (such as copper) is substantial. Therefore the typical CW operating field for a copper cavity is usually kept below 1 MV/m. The microwave surface resistance of a superconductor is typically five orders of magnitude lower than that of copper, and therefore the Q_0 is five orders of magnitude higher. For applications demanding high CW voltage, such as increasing the energy of electron storage rings, the advantage of superconducting cavities becomes clear. Since the dissipated power increases with the square of the operating field, only superconducting cavities can economically provide the needed voltage. For example, LEP requires 2.5

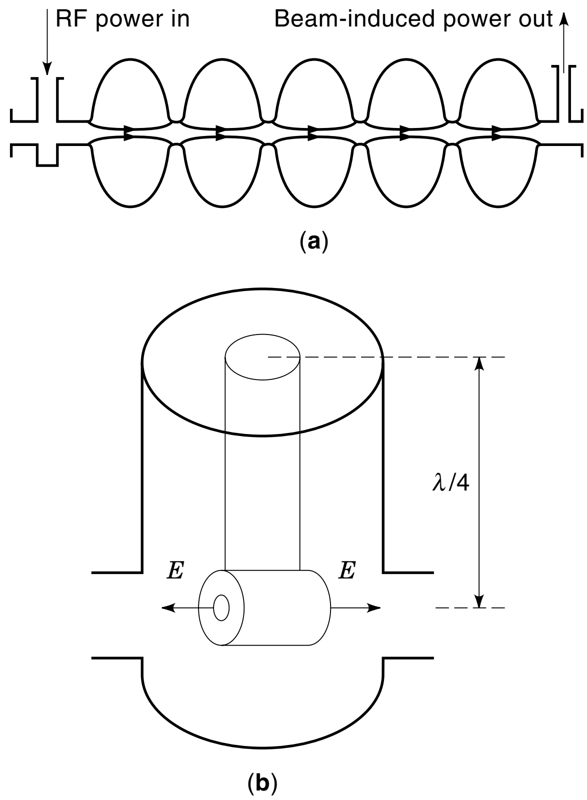

Figure 1. (a). An accelerating structure for velocity of light particles. The resonant frequency for superconducting structures is typically between 350 MHz and 3000 MHz. The cell length is half a wavelength ($\lambda/2$) long. The phase of the electric field on the axis of each cell is shown for the accelerating mode. Ports outside the cell region are for input power couplers and higher-order mode power output couplers. In many applications, the power induced by the beam in higher order modes has to be removed by output couplers. (b) An accelerating structure for low-velocity particles, such as heavy ions. The resonant frequency is typically between 50 MHz and 150 MHz. The accelerating gaps are $\beta_1\gamma_2$ in length, where $\beta = v/c$ and v is the velocity of the heavy ions.

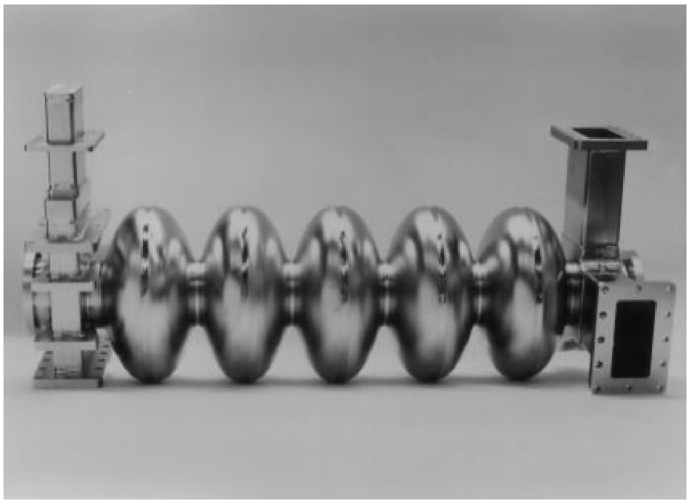

(a)

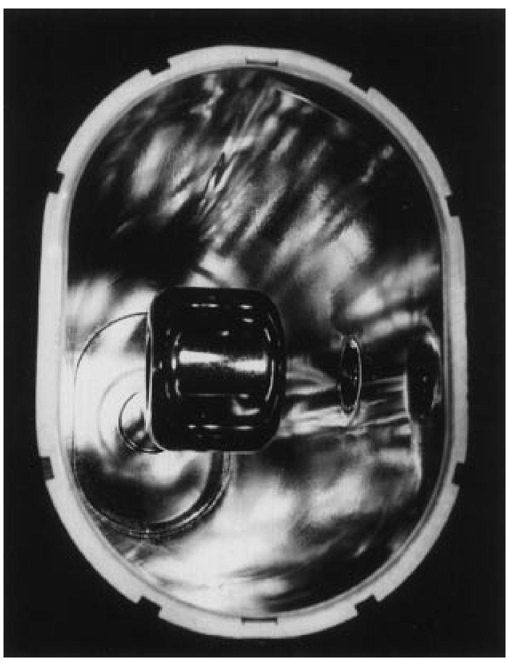

(b)

Figure 2. (a) Five-cell 1.5 GHz niobium cavity developed at Cornell, now used at TJNAF. (b) A quarter-wave resonator from niobium developed for the JAERI (Tokai, Japan) heavy ion linac.

GV to double its energy from 50 GeV to 100 GeV per beam. If copper cavities were to be used, both the capital cost of the klystrons and the ac power operating cost would become prohibitive at the higher accelerating field. Several MW/m of ac power would be required to operate a copper cavity at 5 MV/m. There are also practical limits to dissipating high power in the walls of a copper cavity. When more than 100 kW is dissipated in a copper cell, the surface temperatures exceeds 100°C, causing vacuum degradation, stresses, and metal fatigue due to thermal expansion. High accelerating fields (≈100 MV/m) can be produced in copper cavities, but only for microseconds, and the peak RF power needed (59) becomes enormous (many hundreds of megawatts).

Apart from the general advantages of reduced RF capital and reduced RF associated operating costs, superconductivity offers certain special advantages that stem from the low cavity wall losses. Because of the low power dissipation at high accelerating field, one can afford to make the beam hole of superconducting cavity much larger than for a normal conducting cavity. The large beam hole substantially reduces the beam–cavity interaction [or wake fields (59)], allowing better beam quality and higher current for improving the precision and reaction rates of physics experiments. For the intense proton linacs, where scraping of the proton beam tails is a major worry because of radio-activation of the accelerator, the wide beam hole greatly reduces the risk of beam-loss-induced radioactivity.

RF Superconductivity Basics

The remarkable properties of superconductivity are attributed to the condensation of charge carriers into Copper pairs, which move frictionlessly. At $T = 0$ K, all charge carriers are condensed. At higher temperatures, some carriers are unpaired; the fraction of unpaired carriers increases exponentially with temperature, as $e^{-\Delta/kT}$, until none of the carriers are paired above T_c. Here 2Δ is the energy gap of the superconductor, the energy needed to break up the pairs. In this simplified picture, known as the *London two-fluid model,* when a dc field is turned on, the pairs carry all the current, shielding the applied field from the normal electrons. Electrical resistance vanishes.

In the case of RF currents, however, dissipation does occur for all $T > 0$ K, albeit very small compared to the normal conducting state. While the Cooper pairs move frictionlessly, they do have inertial mass. For high-frequency currents to flow, forces must be applied to bring about alternating directions of flow. Hence an ac electric field will be present in the skin layer, and it will continually accelerate and decelerate the normal carriers, leading to dissipation proportional to the square of the RF frequency. The two-fluid model provides a simple explanation for the quadratic frequency and the exponential temperature dependence of the RF surface resistance. The power dissipated is proportional to the internal electric field (proportional to the RF frequency) and to the normal component of the current. The "normal" component of the current, being proportional to the interior electric field, gives another factor proportional to the RF frequency. The normal component of the current also depends on the number of carriers thermally excited across the gap 2Δ and is given by the Boltzmann factor $e^{-\Delta/kT}$.

Besides the phenomenally low RF surface resistance, other important fundamental aspects are the maximum surface fields that can be tolerated without increasing the microwave surface resistance substantially or without causing a breakdown of superconductivity. The accelerating field, E_{acc}, is proportional to the peak surface RF electric field (E_{pk}), as well as the peak surface RF magnetic surface field (H_{pk}).

The ultimate limit to the accelerating field is the RF critical magnetic field. Theoretically, this is equal to the superheating critical magnetic field. In the Ginzburg–Landau phenomenological theory of superconductivity (7), surface energy considerations lead to estimates for superheating critical field in terms of the thermodynamic critical field, H_c, and the Ginzburg–Landau parameter, κ, as follows:

$$\begin{aligned} H_{sh} &\approx \frac{0.89}{\sqrt{\kappa}} H_c && \text{for } \kappa \ll 1 \\ H_{sh} &\approx 1.2 H_c && \text{for } \kappa \approx 1 \\ H_{sh} &\approx 0.75 H_c && \text{for } \kappa \gg 1 \end{aligned} \quad (1)$$

For the most commonly used superconductor, niobium, H_{sh}, is about 230 mT, which translates to a maximum accelerating field of 55 MV/m for a typical $\beta = 1$ niobium structure and roughly 30 MV/m for a $\beta < 1$ niobium structure.

Typically, cavity performance is, however, significantly below the theoretically expected surface field. One important phenomenon that limits the achievable RF magnetic field is "thermal breakdown" of superconductivity, originating at submillimeter-size regions of high RF loss, called "defects." When the temperature outside the defect exceeds the superconducting transition temperature, T_c, the losses increase, because large regions become normal conducting. Several measures have been developed to overcome thermal breakdown, such as (a) improving the thermal conductivity of niobium by purification or (b) using thin films of niobium (or lead) on a copper substrate cavity.

In the early stages of the development of superconducting cavities, a major performance limitation was the phenomenon of "multipacting." This is a resonant process in which a large number of electrons builds up within a small region of the cavity surface due to the fact that the secondary electron emission coefficient of the surface is greater than unity. The avalanche absorbs RF power, making it impossible to raise the fields by increasing the incident RF power. The electrons impact the cavity walls, leading to a large temperature rise and eventually to thermal breakdown. With the invention of the spherical cavity shape (8) [and later the elliptical cavity shape (9)], multipacting is no longer a significant problem for velocity-of-light structures. Multipacting is still an impediment for structures for low-velocity particles but can be reduced by long periods of exposure to high RF power, called *conditioning,* during which the secondary electron emission is reduced by long-term electron bombardment.

In contrast to the magnetic field limit H_{sh}, there is no known theoretical limit to the tolerable surface electric field. Continuous-wave electric fields up to 145 MV/m (10) and pulsed electric fields up to 220 MV/m (11) have been imposed on a superconducting niobium cavity surface without any catastrophic effects. However, at high electric fields, an important limitation to the performance of superconducting cavities arises from the emission of electrons from high-electric-field regions of the cavity. Power is absorbed by the electrons and deposited as heat when electrons impact the cavity walls. If the emission grows intense, it can even initiate thermal breakdown. There have been extensive studies about the nature of field emission sites as well as development of techniques to avoid emission sites and to destroy them (12).

For low-velocity accelerators, there is an important additional performance consideration. Ambient acoustic noise (microphonics) excites mechanical vibrational modes of the cavity, causing the resonant frequency to vary. The resonant cavities are extended, loaded structures (e.g., drift tubes supported by pipes) and generally have reduced mechanical stability. The cavity RF phase must be synchronized with an RF clock. This requires rapidly tuning the cavity to cancel the effects of acoustically induced mechanical distortions (13).

Figures of Merit for a Superconducting Cavity

We show how to calculate the important physical quantities, such as resonant frequency, accelerating field, peak electric and magnetic fields, power dissipation, quality factor Q_0, and shunt impedance for a simple cavity, the cylindrically symmetric pillbox. The treatment is basic to both normal conducting and superconducting cavities (see CAVITY RESONATORS). We also work out illustrative values. Similar analytic calculations can be carried out for a coaxial TEM quarter wave resonator, as illustrative of an accelerating structure for low-velocity particles. Only simple structures can be calculated analytically. For real structures with beam holes, it is necessary to use field computation codes, such as (a) URMEL (14) for cylindrically symmetric structures and (b) MAFIA (15) for 3-D geometries.

For a cylinder of length d and radius R, the electric (E) and magnetic (H) fields for the standing wave TM_{010} mode are

$$E_z = E_0 J_0\left(\frac{2.405\rho}{R}\right) e^{i\omega t}, \qquad H_\phi = -i\sqrt{\frac{\epsilon_0}{\mu_0}} E_0 J_1\left(\frac{2.405\rho}{R}\right) e^{i\omega t} \quad (2)$$

where all other field components are 0. J_0 and J_1 are Bessel functions of the radial coordinate. The angular resonant frequency $\omega = 2\pi f$ is given by

$$\omega_{010} = \frac{2.405\ \mathrm{c}}{R} \quad (3)$$

Note that the resonant frequency, f, is independent of the cavity length.

Assume an electron traveling nearly at the speed of light (c). It enters the cavity at time $t = 0$ and leaves at a time $t = d/\mathrm{c}$. To receive the maximum kick from the cavity, the time it takes the particle to traverse the cavity is to equal one-half of an RF period, that is,

$$t = \frac{d}{c} = \frac{1}{2} T_{\mathrm{RF}} = \frac{\pi}{\omega} \quad (4)$$

Under this condition, the electron always sees a field pointing in the same direction. The accelerating voltage (V_{acc}) for a cavity is

$$V_{\mathrm{acc}} = \left| \int_{z=0}^{z=d} E_{\mathrm{el}}\, dz \right| \quad (5)$$

For an electron accelerator with energy > 10 MeV, it is sufficiently accurate to use $v = c$, so that $t(z) = z/\mathrm{c}$. Thus

$$V_{\mathrm{acc}} = \left| \int_{z=0}^{z=d} E_z(\rho = 0, z) e^{i\omega z/\mathrm{c}}\, dz \right| \quad (6)$$

$$V_{\mathrm{acc}} = E_0 \left| \int_{z=0}^{z=d} e^{i\omega z/\mathrm{c}}\, dz \right| = dE_0 \frac{\sin\left(\frac{\omega d}{2\mathrm{c}}\right)}{\frac{\omega d}{2\mathrm{c}}} = dE_0 T \quad (7)$$

Here T is referred to as the "transit time factor." At 1.5 GHz we have $d = c\pi/\omega = 10$ cm, and Eq. (7) simplifies to

$$V_{\mathrm{acc}} = 0.064\ \mathrm{m} \cdot E_0$$

The average accelerating electric field (E_{acc}) is given by

$$E_{\mathrm{acc}} = \frac{V_{\mathrm{acc}}}{d} = \frac{2E_0}{\pi} \tag{8}$$

Here E has the dimensions of V/m.

Peak Surface Fields

To achieve a high accelerating field in a cavity, it is important to minimize the design ratios of the peak fields to the accelerating field. For the TM_{010} mode in a pillbox cavity we have

$$E_{\mathrm{pk}} = E_0, \qquad H_{\mathrm{pk}} = \sqrt{\frac{\epsilon_0}{\mu_0}} J_1(1.841) E_0 = \frac{E_0}{647\Omega} \tag{9}$$

Thus we obtain the following ratios:

$$\frac{E_{\mathrm{pk}}}{E_{\mathrm{acc}}} = \frac{\pi}{2} = 1.6, \quad \frac{H_{\mathrm{pk}}}{E_{\mathrm{acc}}} = 2430\ \frac{\mathrm{A/m}}{\mathrm{MV/m}} = 3.05\ \frac{\mathrm{mT}}{\mathrm{MV/m}} \tag{10}$$

The units for magnetic field used are teslas.

Power Dissipation and Q_0

In order to support the electromagnetic fields, currents flow within a thin surface layer of the cavity walls. If the surface resistance is R_s, the power dissipated/unit area (P_a) due to Joule heating is

$$P_a = \frac{1}{2} R_s H^2 \tag{11}$$

The quality, Q_0, is related to the power dissipation by the definition of Q_0:

$$Q_0 = \omega \frac{\text{Energy stored}}{\text{Power dissipated}} = \frac{\omega U}{P_c} \tag{12}$$

where U is the stored energy and P_c is the dissipated power.

The total energy in the cavity and the power dissipated are

$$U = \frac{1}{2}\mu_0 \int_v |H|^2\, dv, \qquad P_c = \frac{1}{2} R_s \oint_s |H|^2\, d\mathbf{s} \tag{13}$$

where the integral is taken over the volume of the cavity. Thus

$$Q_0 = \frac{\omega\mu_0 \int_v |H|^2\, dv}{R_s \oint_s |H|^2\, d\mathbf{s}}, \qquad Q_0 = \frac{G}{R_s}, \qquad G = \frac{\omega\mu_0 \int_v |H|^2\, dV}{\oint_s |H|^2\, d\mathbf{s}} \tag{14}$$

Here G is called the *geometry factor*. It only depends on the cavity shape and not its size. For the TM_{010} mode in a pillbox cavity, we obtain

$$U = \frac{\pi\epsilon_0 E_0^2}{2} J_1^2(2.405)\, dR^2 \tag{15}$$

$$P_c = \frac{\pi R_S E_0^2 \epsilon_0}{\mu_0} J_1^2(2.405) R[R+d] \tag{16}$$

$$G = \frac{453Rd}{(R^2 + Rd)}\ \Omega \tag{17}$$

Combining Eqs. (3) and (4), we find that in order to obtain the maximum accelerating voltage from the cavity, we require

$$\frac{R}{d} = \frac{2.405}{\pi} \tag{18}$$

so that $G = 257\ \Omega$. A typical observed surface resistance for a well-prepared superconducting Nb cavity is $R_s = 20\ \mathrm{n}\Omega$. Thus we have a Q_0 value of

$$Q_0 = \frac{G}{R_s} = 1.3 \times 10^{10} \tag{19}$$

For a typical cavity length of $d = 10$ cm (at 1.5 GHz), we obtain $R = 7.65$ cm. For an accelerating voltage of 1 MV, we obtain the following results:

$$\begin{aligned} E_{\mathrm{acc}} &= \frac{V_{\mathrm{acc}}}{d} = 10\ \mathrm{MV/m} \\ E_{\mathrm{pk}} &= E_0 = \frac{\pi}{2} E_{\mathrm{acc}} = 15.7\ \mathrm{MV/m} \\ H_{\mathrm{pk}} &= 2430 \frac{\mathrm{A/m}}{\mathrm{MV/m}}\, E_{\mathrm{acc}} = 24.3\ \mathrm{kA/m} = 30.5\ \mathrm{mT} \\ U &= \frac{\pi\epsilon_0 E_0^2}{2} J_1^2(2.405)\, dR^2 = 0.54\ \mathrm{J} \\ P_c &= \frac{\omega U}{Q_0} = 0.4\ \mathrm{W} \end{aligned} \tag{20}$$

The performance of a superconducting cavity is evaluated by measuring the Q_0 as a function of the cavity field level. This gives information on the average behavior of the RF surface.

Thermometry Based Diagnostics

To resolve the local distribution of RF losses from various mechanisms described above, temperature mapping is used as a diagnostic technique. A chain of rotating carbon thermometers, or an array of fixed thermometers, samples the temperature of the outer wall of the cavity. Temperature mapping with carbon thermometers has played a key role in improving the understanding of mechanisms that lead to residual resistance, multipacting, thermal breakdown, and field emission. Carbon makes a sensitive thermometer at liquid helium temperatures because, as a semiconductor, its resistance increases exponentially with decreasing temperature. Above the superfluid temperature (2.17 K), temperature increments of the cavity wall of a few mK can be easily detected. A single rotating arm bearing 10 to 20 thermometers per cell is appropriate for locating stable field emitters or thermal defects in sizable structures, such as a multicell cavity. For temperature mapping in superfluid helium, thermometers need to be isolated from the superfluid bath so that movable elements do

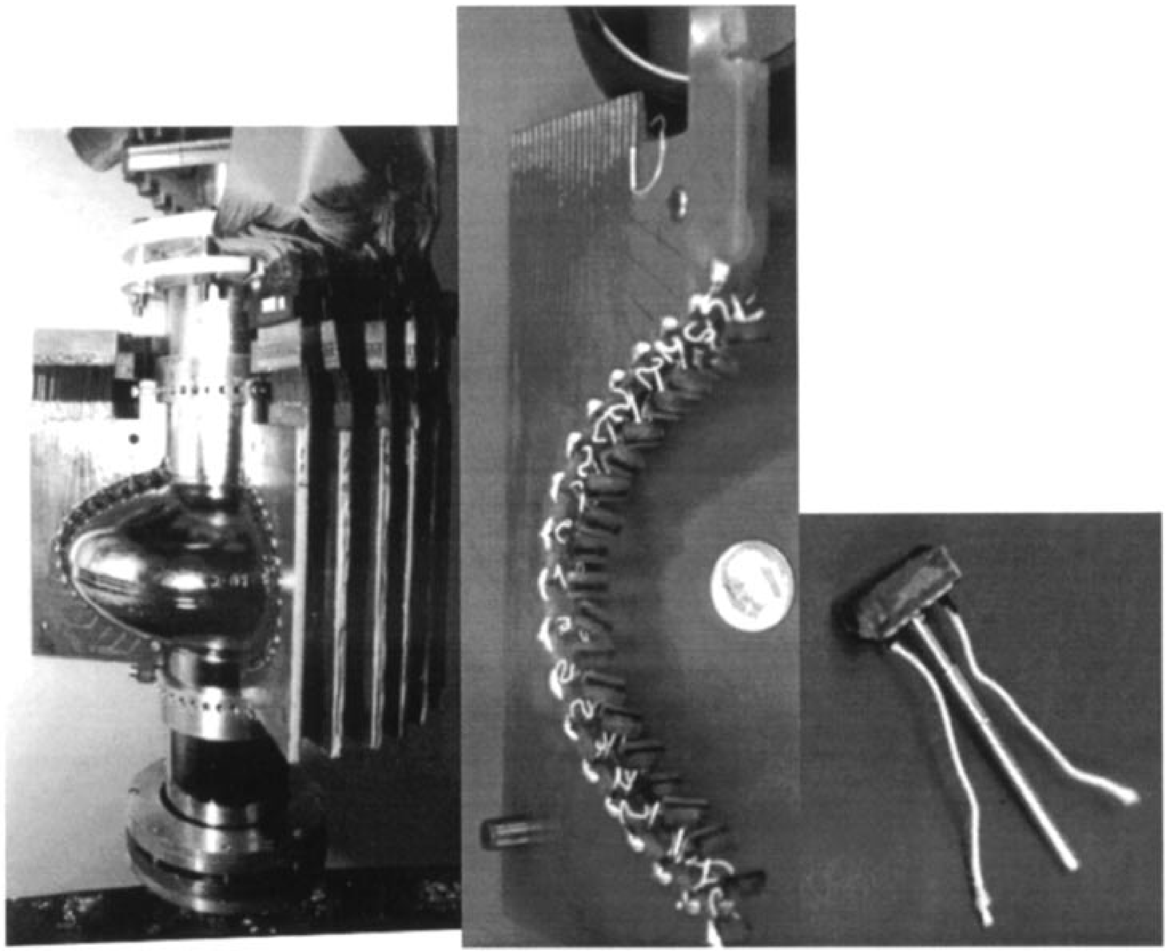

(a) (b) (c)

Figure 3. (a) A single-cell niobium cavity surrounded by an array of ≈700 carbon thermometers that make close contact with the outer wall of the cavity. (b) There are 19 thermometers placed on each individual board that is contoured to closely follow the cavity profile. (c) A single thermometer consists of a 100 Ω carbon resistor embedded in an epoxy housing. It is held by a spring-loaded pin inserted into holes in the board. The surface of the thermometer is ground so that the carbon element is exposed and subsequently covered with a thin layer of varnish to provide electrical insulation. The leads are made of a low-thermal-conductivity alloy, such as manganin.

not provide good sensitivity. A large array of fixed thermometers is preferred. These are brought in intimate contact with the cavity wall by the use of spring loaded contacts. Grease applied between the cavity wall and the thermometer element improves heat transfer and keeps the superfluid away. Due to the large number of thermometers and leads, the fixed method is suitable for investigations with single cell cavities. An example of a fixed thermometry system is shown in Fig. 3, and a typical temperature map is shown in Fig. 4 (16).

Refrigerator Requirements

Although the power dissipated in the superconducting cavity is very small, the losses will be dissipated in the liquid He bath. Together with the static heat leak to the cryostat, these losses comprise the cryogenic loss. Typically the ac power needed to operate the refrigerator is larger than the dissipated power in 2K liquid He by a factor of 750. One part of this factor comes from the technical efficiency (η) of the refrigerator, typically $\eta = 0.2$ for a large system, and the other part

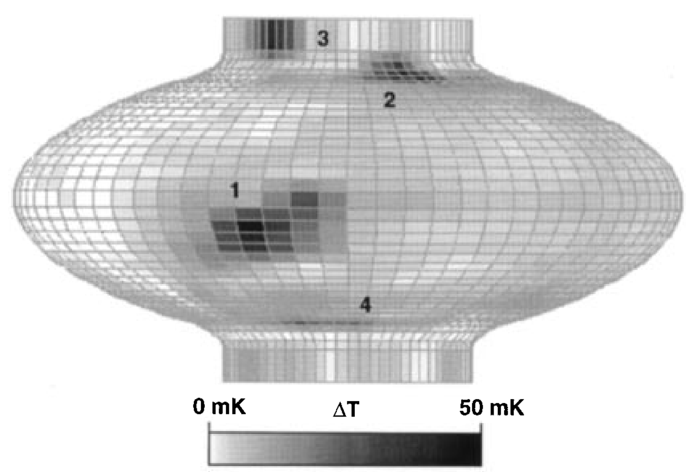

Figure 4. Temperature map at 40 mT of a single-cell 1.5 GHz cavity showing heating at a defect site near the cavity equator (labeled 1) and field emission sites (labeled 2, 3, and 4) near the cavity iris.

comes from the Carnot efficiency η_c, which at 2 K is

$$\frac{1}{\eta_c} = \frac{300-2}{2} \tag{21}$$

At 10 MV/m the required refrigerator ac power due to the RF loss would be 300 W for the case of a single-cell 1.5 GHz cavity. For a copper cavity of the same geometry, with a typical R_s = 3 mΩ, the RF power dissipation in the cavity would be 60 kW for an accelerating field E_{acc} = 10 MV/m. Furthermore, the ac wall power will be a factor of 2 higher because of the typical klystron efficiency. Thus the ac power cost of running a copper cavity in CW mode would be several hundred times higher than the cost for an Nb cavity.

Shunt Impedance

An important quantity used to characterize the losses in a cavity at a given accelerating voltage is the shunt impedance (R_a) as typified by a parallel *RLC* circuit:

$$R_a = \frac{V_{acc}^2}{P_c} \tag{22}$$

in which case P_c = power dissipated and V_{acc} is the acceleration voltage. Hence the shunt impedance is in ohms.

Ideally the shunt impedance should be large for the accelerating mode so that the dissipated power is small. This is particularly important for copper cavities, where the wall power dissipation is a major issue and we wish to have as large an accelerating field as possible. For the TM_{010} mode pillbox cavity and R_s of 20 nΩ we have

$$R_a = \frac{4\mu_0 d^2}{\pi^3 R_s \epsilon_0 J_1^2(2.405)R[R+d]} = 2.5\times 10^{12}\ \Omega \tag{23}$$

Note that the ratio of R_a/Q is given by

$$\frac{R_a}{Q_0} = \frac{V_{acc}^2}{\omega U} \tag{24}$$

which is independent of the surface resistance. For the pillbox TM_{010} mode we have

$$\frac{R_a}{Q_0} = 150\,\Omega\frac{d}{R} = 196\,\Omega \tag{25}$$

By applying computer codes to determine electromagnetic fields, the computed figures of merit for the Cornell/TJNAF 5-cell cavity are given in Table 1. Note that due to the presence of the beam holes the shunt impedance is reduced and the peak surface fields are enhanced, relative to the pillbox case. For a realistic cavity shape, R/Q_0 is lowered due to the presence of the beam holes, typically by a factor of 2.

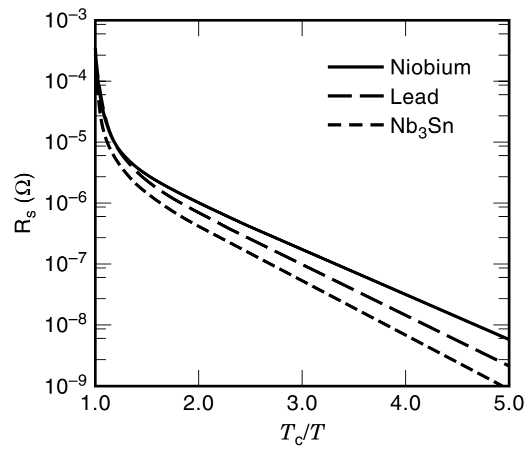

Figure 5. Theoretical surface resistance at 1.5 GHz of lead, niobium, and Nb_3Sn as calculated from Halbritter's program (20). The values used for the material parameters are given in Table 2.

RF Surface Resistance

Based on the very successful BCS theory (17), expressions for the superconducting surface impedance have been worked out by Mattis and Bardeen (18). These expressions involve material parameters, such as the London penetration depth λ_L, the coherence distance ξ_0, the Fermi velocity V_F, and the electron mean free path l. They are in a rather difficult form to obtain general formulas to work with. Computer programs have been written—for example, by Turneaure (19) and Halbritter (20). Figure 5 gives the results from Halbritter's programs for niobium and lead and Nb_3Sn. Table 2 gives the material parameters used for the calculations. Calculations from the theory agree well with experimentally measured R_s for $T/T_c >$ 0.3. At lower temperatures the residual resistance term dominates.

A simplified form of the temperature dependence of Nb for $T_c/T > 2$ and for frequencies much smaller than $2\Delta/h \approx 10^{12}$ Hz is

$$R_s = A(1/TJ)f^2\exp(-\Delta(T)/k_BT) + R_0 \tag{26}$$

Here k_B is Boltzmann's constant. The second term, R_0, is called the *residual resistance.* Typical R_0 values for Nb cavities fall in the range from 10^{-7} to 10^{-8} Ω. The record for the lowest surface resistance is 1–2 × 10^{-9} Ω (21). For comparison, the surface resistance of copper at 1.5 GHz is 3 mΩ.

Table 1. Figures of Merit for the Cornell/CEBAF 5-Cell Cavity

G	290 Ω
R/Q (per 5-cell cavity)	480 Ω
E_{pk}/E_{acc}	2.6
H_{pk}/E_{acc}	4.7 MT/(MV/m)

[a]Data taken from Ref. 4.

Table 2. Material Parameters Used for the Calculations of Fig. 5

Material Parameter	Pb	Nb	Nb_3Sn
T_c [K]	7.19	9.20	18.00
Energy gap, Δ/kT_c	2.10	1.86	2.25
Penetration depth λ [Å]	280	360	600
Coherence length ξ [Å]	1110	640	60
Mean free path ℓ [Å]	10,000	500	10

The operating temperature of a superconducting cavity is usually chosen so that the first term in Eq. (26) is reduced to an economically tolerable value. R_0, referred to as the *residual resistance,* is influenced by several factors. Some of the sources are extraneous to the superconducting surface—for example, lossy joints between components of the structure. Other factors originate at the superconducting surface. A well-understood and controllable source of residual loss is trapped dc magnetic flux from insufficient shielding of the earth's magnetic field, or other dc magnetic fields in the vicinity of the cavity. To get the highest Q_0, a superconducting cavity must be well-shielded from the earth's field. Typically, at 1 GHz, R_0 is 10 $\mu\Omega$/mT (22). Another important residual loss mechanism arises when the hydrogen dissolved in bulk niobium precipitates as a lossy hydride at the RF surface (23). This residual loss is a subtle effect that depends on the rate of cooldown and the amount of other interstitial impurities present in niobium. The effect can be severe enough to lower the Q_0 to 10^8 depending on the amount of hydrogen dissolved and the cooldown rate of the cavity. More than 2 ppm wt of hydrogen can be dangerous.

Cavity Fabrication and Surface Preparation

Niobium cavities can be constructed from sheet niobium using the techniques of forming (e.g., deep drawing or spinning) followed by electron beam welding (24). Another method is to deposit a thin niobium film onto a preformed copper cavity substrate (25). The copper cavity is made in essentially the same way as the sheet niobium cavity, except for surface preparation before film deposition. If the cavity has more than one cell, the cells need to be tuned relative to each other, by adjusting the dimensions, so that the accelerating field is the same for each cell. Dimensional variations between cells are sufficient to alter the field profile substantially. Typical fabrication tolerances are in the range of a few tenths of a millimeter.

The purity of niobium used is important, both in terms of bulk impurity content and in terms of inclusions from manufacturing steps, such as rolling. Inclusions on the RF surface play the role of normal conducting sites for thermal breakdown. Dissolved impurities serve as scattering sites for the electrons not condensed into Cooper pairs. These impurities lower the thermal conductivity, impede the heat transfer to the helium, and limit the maximum tolerable surface magnetic field before the onset of thermal breakdown. The accompanying decrease in electrical conductivity, or the *RRR* value, serves as a convenient measure of the purity of the metal. The formal definition of *RRR* is

$$RRR = \left(\frac{\text{resistivity at 300 K}}{\text{residual resistivity at low temperature (normal state)}} \right) \tag{27}$$

Here low temperature means the temperature at which the dc resistivity in the normal state becomes residual. A convenient relationship between thermal conductivity and *RRR* for niobium is

$$k \approx 0.25\, RRR \left(\frac{\mathrm{W}}{\mathrm{mK}} \right) \tag{28}$$

This relationship can be derived from the Wiedemann–Franz law (26) and from the ratio of the superconducting to normal conducting state thermal conductivities (27). To achieve the optimum RF performance, the surface of the cavity must be prepared to approach as close as possible the ideal. Microscopic contaminants can limit the performance, either by thermal breakdown or by field emission (28). A clean RF surface is achieved by chemically etching away a surface layer, rinsing thoroughly with ultraclean water, and then taking precautions so that no contaminants come in contact with the clean RF surface. The resistivity of the water should be close to theoretically pure (18 MΩ-cm), and the water should be filtered to eliminate particles larger than 1 μm. After etching, water is recirculated for several hours through the cavity in series with the water purification system so as to continuously and thoroughly remove any chemical and particulate residue from the niobium surface. For a review of cavity fabrication and preparation procedures, see Ref. 28.

Many laboratories have found that the RF surface can be made even cleaner if chemistry is followed by high-pressure rinsing (HPR) of the cavity with ultrapure water (29). At TJNAF for example, water at a pressure of 70 bar to 80 bar is sprayed through stainless steel nozzles each having a 0.3 mm diameter orifice (30). The potent jets of water are scanned across all parts of the RF surface to dislodge and sweep away microscopic contaminants that have adhered to the surface.

After rinsing, the cavity is transported into a dust-free clean room where the water is drained. The cavity surface thus only comes in contact with filtered air. The level of cleanliness required is comparable to that in the semiconductor industry where a clean room environment of Class 10–100 is routine. Class 10 refers to the number of particles of size 0.5 microns or larger in one cubic foot of air. The surface of the cavity must be dried before the cavity is evacuated, placed inside a cryostat, and cooled down for RF tests. During final assembly, the laboratory workers in the vicinity need to wear special particulate-free clothing and follow strict protocols to reduce particulate generation.

During these various stages of cavity production and preparation, there are many opportunities for defects to enter the cavity. Therefore great care must be exercised during the manufacture of sheet metal, deep drawing of cups, electron beam welding, chemical etching, rinsing, drying, and insertion of coupling devices, as well as in the final attachment of the cavity to the vacuum system of the test stand or the accelerator. Two examples of defects that caused thermal breakdown are shown in Fig. 6 (31). On a statistical basis, we expect that the number of defects increases with cavity surface area.

Overcoming Field Emission

The temperature mapping diagnostic technique for superconducting cavities shows that emission arises from particular spots, called "emitters," located in high-electric-field regions. The electrons that emerge from the emitters travel in the RF fields of the cavity and impact the surface (Fig. 7). Some electrons may be captured in the axial fields and accelerated along with the beam. These produce unwanted "dark current," which may spoil the beam quality or impact the walls of adjacent cavities. The pattern of temperature rise as a function of position along a given meridian contains implicit

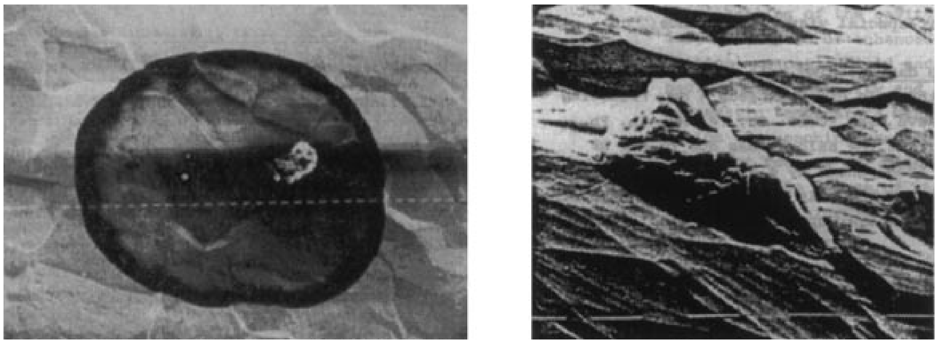

(a) (b)

Figure 6. SEM micrographs of defects that caused thermal breakdown. (a) A chemical or drying stain 440 μm in diameter. The small crystal on the right side contains K, Cl, and P. This defect quenched at E_{acc} = 3.4 MV/m. (b) A 50 μm crystal containing S, Ca, Cl, and K. This defect quenched at E_{acc} = 10.7 MV/m. These defects were located by temperature maps. (Courtesy of CERN.)

information about the location and characteristics of the source. The power deposited by the impacting electrons depends on the trajectory as well as on the intrinsic properties of the emitter.

In their basic theory of field emission (32), Fowler and Nordheim (FN) showed that in the presence of an electric field, electrons tunnel out of the metal into the vacuum because of their quantum wave-like nature. However, a comparison with the observed currents reveals that, at a given field, emission is substantially higher than the FN predictions. Traditionally, the excess has been attributed to a "field enhancement factor," which is believed to be related to the physical properties of the emitter discussed below. Both RF and dc studies reveal that emitters are micron- to sub-micron-size contaminant particles (13). Figure 8 shows an example of a region of emitting particles found in a niobium cavity (33). The properties of the emitter that lead to enhanced emission are (a) the microgeometry of the particle (34), (b) the nature of condensed gases or adsorbates on the surface of the particle (35), and (c) the interface between the particle and the underlying metal RF surface (36). Accordingly, a high level of cleanliness is necessary for cavity surface preparation. Field emission free performance has been achieved with HPR (30). Recently, many 9-cell 1.3 GHz structures were prepared at

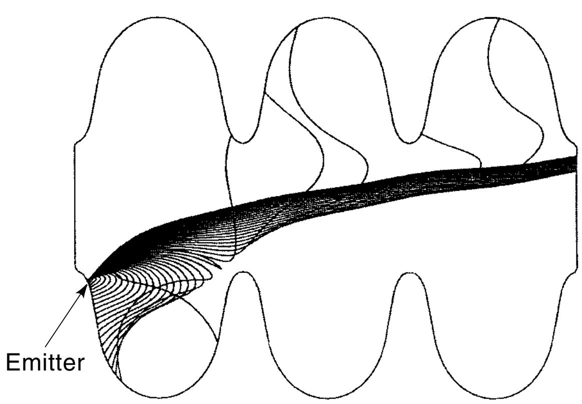

Figure 7. Calculated electron trajectories in a 3-cell 1.5 GHz cavity operating at E_{pk} = 50 MV/m. The emitter is located in the end cell, where the surface electric field is 44 MV/m. Note that a significant number of field-emitted electrons bend back and strike the wall near the emitter. Others are accelerated through the cavity structure and could produce unwanted "dark current" that may be accelerated in adjacent cavities.

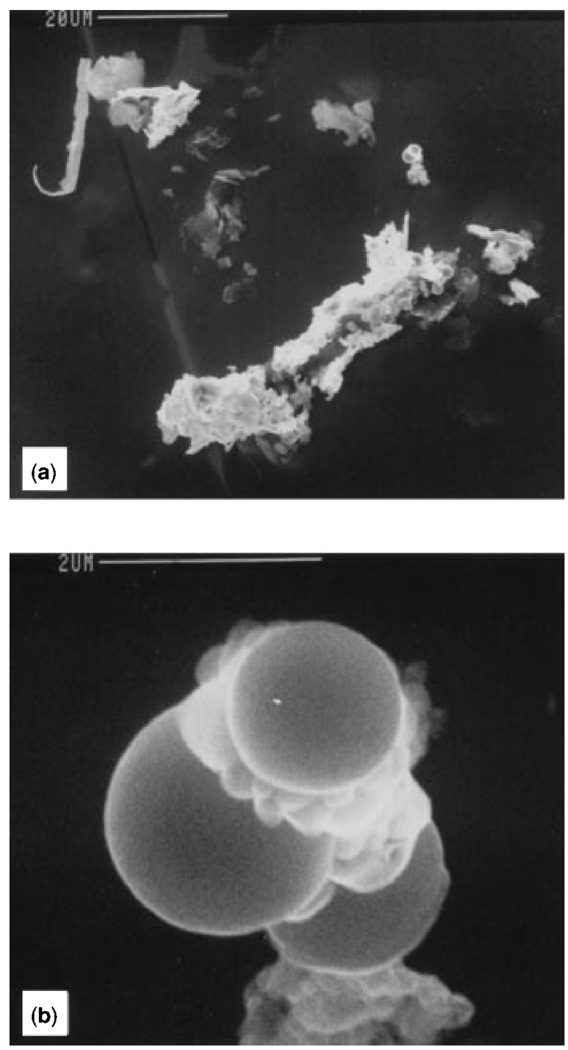

Figure 8. (a) SEM micrograph of field emitting particles. Note the cluster of small spherical balls which indicate that a part of the site melted. EDX analysis shows that the particles are stainless steel. Note also the jagged microgeometry of the particles believed responsible for field enhancement. (b) The melted cluster is expanded.

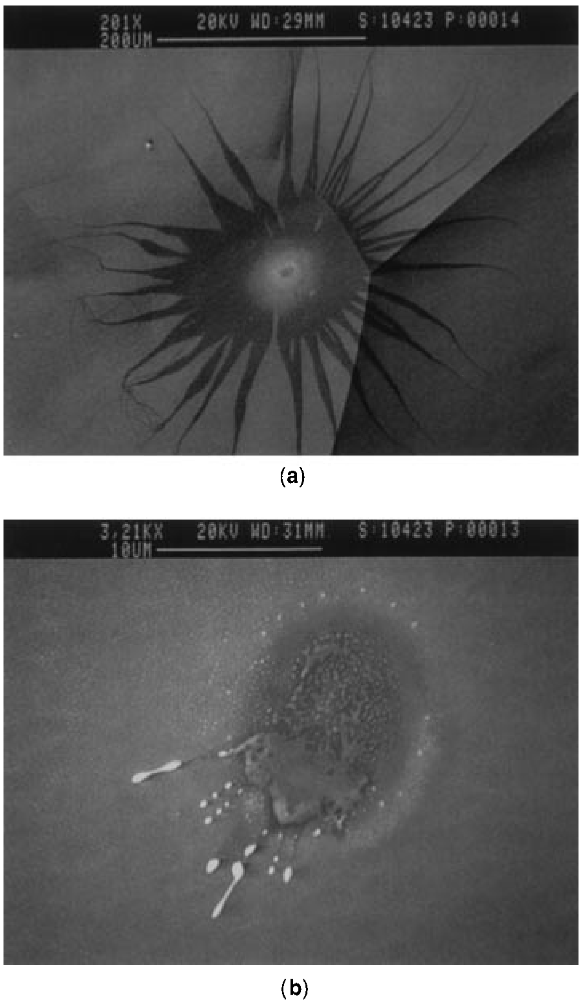

Figure 9. SEM pictures of the processed site found at the location predicted via temperature maps. (a) Low magnification; (b) high magnification of crater region within the starburst of (a). The molten splashes in the crater region were found to contain indium, presumably from the indium wire seals used to make vacuum joints.

DESY by using HPR (37). A sample of their results is shown in Fig. 11.

When raising the RF electric field in a superconducting cavity for the first time, the field emission often decreases abruptly; the cavity is said to "process" or "condition." There has been much progress in characterizing processed emitters at a microscopic level using techniques such as SEM, EDX, Auger, and AFM. These studies reveal that emitter processing is an explosive event that accompanies what we usually refer to as a "spark" or a "discharge," or the "electrical breakdown" of the insulating vacuum (38). Figure 9 shows a typical SEM micrograph of an exploded emitting site (39).

To reach the highest accelerating fields, the highest thermal conductivity is essential to avoid thermal breakdown, and a high level of cleanliness is essential to avoid field emission. High-pressure water rinsing is a very successful cleaning technique to avoid field emission. In multicell structures with large surface area, there is always a significant probability that a few emitters will eventually find their way on to the cavity surface. There is also the danger of dust falling into cavities during installation of power coupling devices as well as during installing of the structure into the accelerator.

A technique that eliminates field emitters *in situ* is high pulsed power RF processing (HPP) (40). The essential idea is to raise the surface electric field at the emitter as high as possible, even if for a very short time ($\ll$ milliseconds). As the field rises, the emission current rises exponentially to the level at which melting, evaporation, gas evolution, plasma formation, and ultimately a microdischarge (RF spark) take place. The ensuing explosive event destroys the emitter. An important benefit of HPP is that the technique can be applied to recover cavities after their final installation. It can also be used to recover the performance of cavities which may be accidentally contaminated, as, for example, in a vacuum mishap. To achieve emission-free performance at a desired E_{acc}, processing must be carried out at $\approx 2 \times E_{acc}$. Figure 10 shows the improvement in performance achieved by HPP (41). [Recently, many 9-cell 1.3 GHz structures were prepared at DESY by using HPR techniques (37). A sample of their results is shown in Fig. 11. Occasionally it is possible to achieve field emission free performance, as shown by the best curve of Fig. 11.]

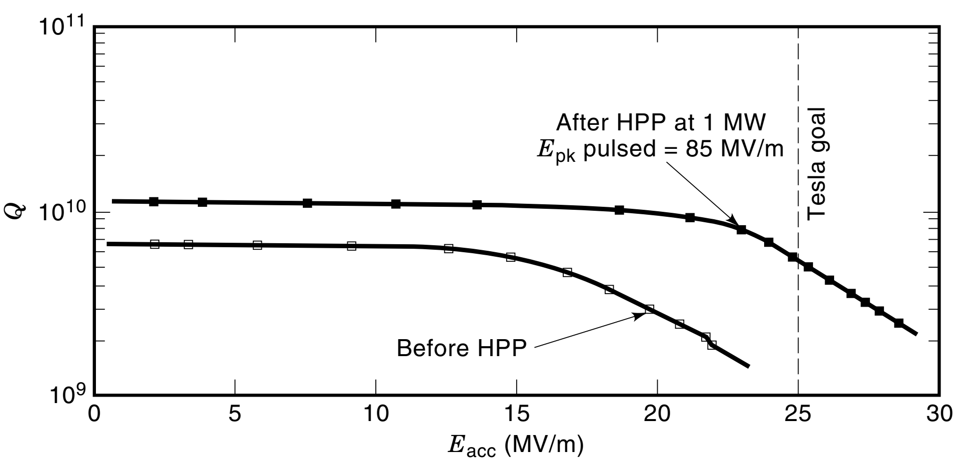

Figure 10. Performance of a 5-cell 1.3 GHz niobium cavity improved by HPP. Before HPP, the maximum field was limited by heavy field emission to E_{acc} = 22 MV/m. After applying 1 MW of power and reaching E_{pk} = 90 MV/m in the pulsed mode, the field emission was processed away and E_{acc} = 28 MV/m was possible in the CW mode.

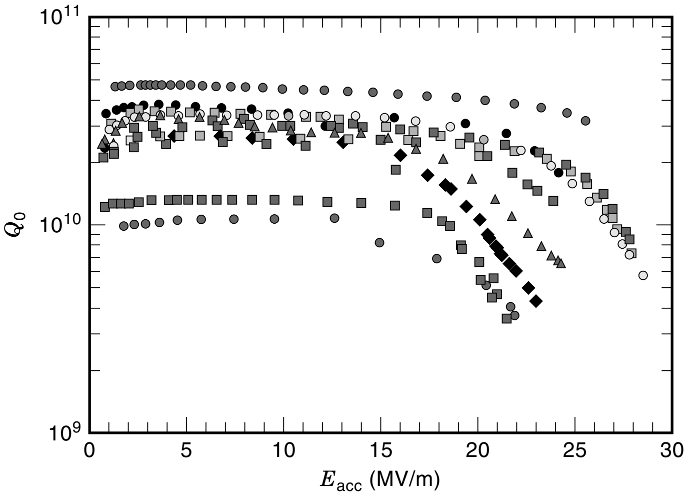

Figure 11. High performance of several 9-cell 1.3 GHz cavities achieved by high-pressure rinsing.

Overcoming Thermal Breakdown

The most effective cure for thermal breakdown caused by millimeter- to submillimeter-size defects is to (a) use better quality material that is free of such defects or (b) to raise the thermal conductivity of the niobium so that remaining defects will be able to tolerate more power before driving the neighboring superconductor into the normal state (42). A simple analysis of the thermal breakdown shows that the maximum magnetic surface field is given by

$$H_{\max} = \sqrt{\frac{4k(T_c - T_b)}{aR_n}}, \quad \text{i.e.,} H_{\max} \propto \sqrt{k} \propto \sqrt{RRR} \qquad (29)$$

Here k is the thermal conductivity, T_c is the superconducting transistor temperature, T_b is the bath temperature, a is the radius of the defect, and R_n is the surface resistance of the defect. This dependence on *RRR* is supported by detailed numerical simulations of thermal breakdown, as well as by experiments on cavities made from Nb of different *RRR* (Fig. 12).

Figure 13 shows the thermal conductivity of three samples of niobium that have different histories of heat treatment (43). The common feature of all three curves is the sharp drop below T_c = 9.2 K, as more and more electrons condense into Cooper pairs. At the higher temperatures (4 K $< T < T_c$), a significant, though small, fraction of electrons is not frozen into Cooper pairs and can carry heat effectively, provided that the electron-impurity scattering is low. Since the temperature in the neighborhood of the defect is between the bath temperature and T_c, the high-temperature thermal conductivity is the most important and has the strongest effect on thermal breakdown. The higher the *RRR*, the higher the thermal conductivity in this temperature range.

Below 4 K, as electrons condense into Cooper pair, electron–phonon scattering also decreases. As a result, the thermal conductivity from phonons begins to increase, leading to the phonon peak near 2 K. With decreasing temperature, the number of phonons decreases ∝ T^3, The value of the phonon conductivity maximum is limited by phonon scattering from

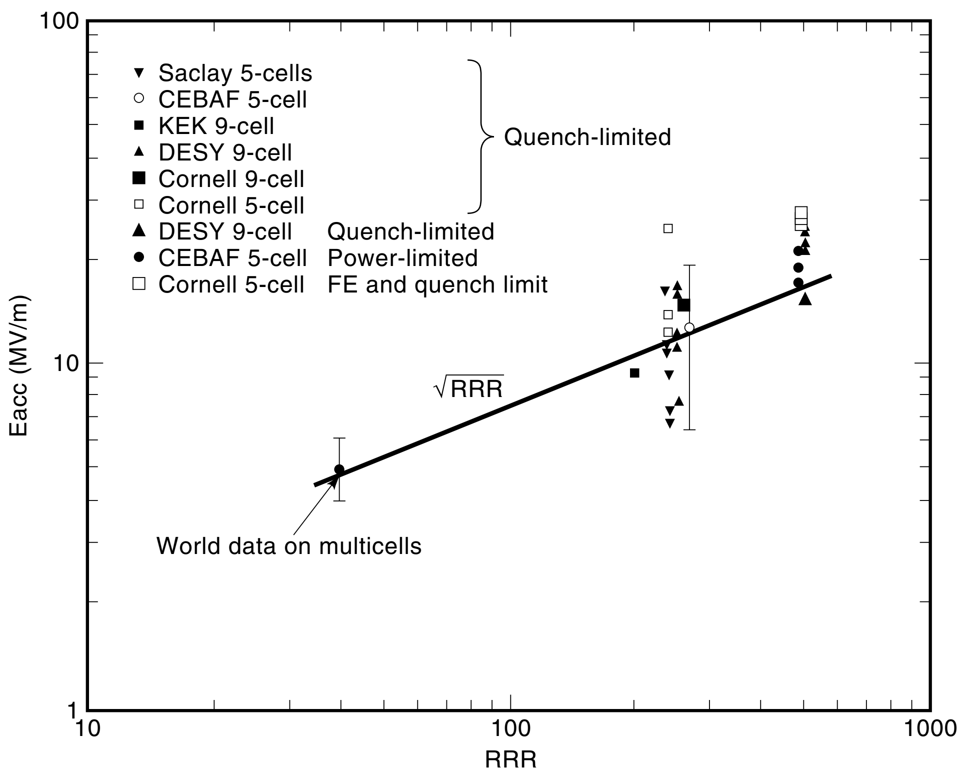

Figure 12. A summary of the results of multicell cavities [(39–43) showing the importance of high *RRR* coupled with emission reduction techniques such as HPP and HPR. The line shows a $\sqrt{RRR}$ dependence expected from the simple theory of thermal breakdown.

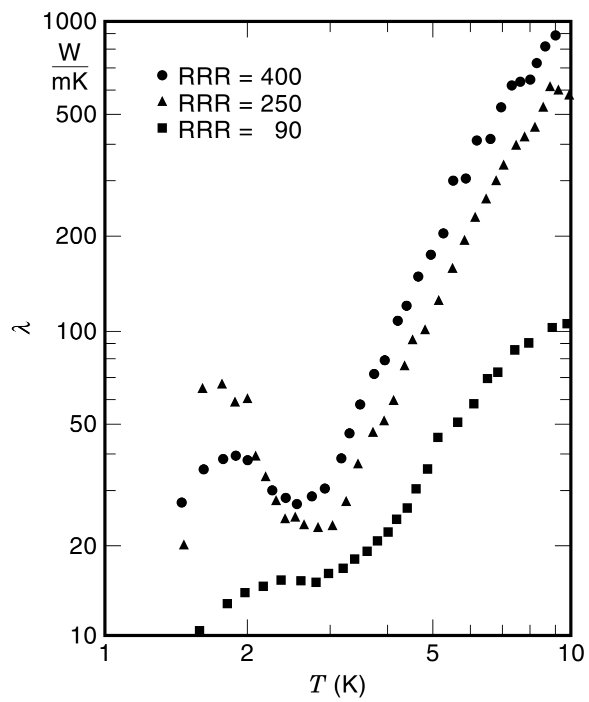

Figure 13. Thermal conductivity (λ) of niobium with RRR = 90 (as received), RRR = 400 after post-purification with yttrium, and RRR = 250 after annealing the post-purified sample for 6 hours at 1400°C. (Courtesy of Wuppertal.)

lattice imperfections, of which the grain boundary density is the most important. If the crystal grains of niobium are very large (e.g., because of annealing at high temperature), one observes a large phonon peak, as shown in the thermal conductivity behavior of the sample with RRR = 250, which was annealed at 1400°C. Since the phonon peak is at about 2 K, it does not help to thermally stabilize defects that heat up in the RF field.

The light, interstitially dissolved impurities have the strongest effect on the RRR. Among these, oxygen is dominant. The other interstitials are carbon, nitrogen, and hydrogen. Among the metallic impurities, tantalum is found in the highest concentration (typically 500 ppm by weight) since all naturally occurring ores contain some tantalum. This impurity level is not a problem since tantalum is a substitutional impurity and does not substantially affect the electronic properties. However, Ta can become a problem if clustering occurs. The Nb used to fabricate a cavity has been checked, for example, by an eddy current scanning technique (44) to look for large defects such as Ta clusters. Next in abundance are the higher-temperature, refractory elements, such as tungsten, zirconium, hafnium, and titanium, usually found at the level of 10–50 ppm wt. The electron-scattering effectiveness of the various impurities are shown in Table 3 in terms of their effect on the RRR (45).

To obtain the net RRR, one must add the resistance contributions for each impurity element in parallel. The contributions of the phonons is always present, so that the highest theoretical RRR for niobium is 35,000 (46). Experimentally, the highest RRR ever achieved in a niobium sample was 28,000 (47).

The most convenient method to obtain high-purity niobium for superconducting cavities is to remove the interstitials during the electron-beam melting stages of the ingot. Multiple melts and progressive improvements in the furnace chamber vacuum have led to a steady increase in the RRR of commercial niobium over the last decade from 30, typical of commonly available “reactor grade” niobium, to 300 (48). The RRR of commercially available Nb continues to improve. Recently, niobium sheet of RRR = 500–700 became available from a Russian source (49).

If RF surface magnetic fields higher than 50 mT are desired on a consistently reproducible basis, the thermal conductivity of the niobium must be improved to $RRR > 300$. In one method called *post-purification,* the purity of the niobium is increased by solid-state gettering of oxygen using yttrium (50) or titanium (51) at high temperature. The foreign metal is vapor-deposited on the niobium surface. In the same step, the high temperature decreases the diffusion time of the oxygen in niobium. Over a few hours, oxygen is trapped in the deposited getter layer. If yttrium is used, the best temperature is 1200–1250°C because both the vapor pressure of yttrium and the diffusion rate of oxygen in niobium are sufficiently high. If titanium is used, temperatures of 1350–1400°C are required because of the lower vapor pressure of titanium. Typically during post-purification, the RRR improves by a factor of two in a few hours. An important disadvantage of the post-purification is that the yield strength of niobium falls substantially due to the high-temperature treatment. Also, titanium diffusion into the bulk along grain boundaries demands additional etching.

Nb/Cu Cavities

As we mentioned, thin Nb films on higher-thermal-conductivity copper is another way to avoid thermal breakdown. The technique of sputter coating niobium has been developed by CERN for 350 MHz structures and applied successfully to hundreds of structures (25). In the most successful coating method to date, thin film deposition is carried out by cylindrical magnetron sputtering. Before the coating stage, the copper cavity is degreased, chemically polished (≈ 20 μm), rinsed with high-purity, dust-free water and alcohol, and dried under clean laminar air flow. After bakeout of the copper cavity to reach a good vacuum, a typical coating time is 4 hours. The coating thickness is a few microns at a substrate temperature of 180–200°C. The RRR of the deposited niobium serves as one of the monitors of film quality. The sputtering rate and substrate temperature are optimized to reach an RRR greater than 20. Note that the low RRR relative to bulk niobium is not a problem because the film is very thin. The rod-like grains of the niobium film are up to 1 μm long and 10–150

Table 3. Expected *RRR* for 1 ppm wt of Major Impurities[a]

Element	*RRR*
H	2640
N	4230
C	4380
O	5580
Ta (1000 ppm wt)	1140

[a]Note that the effect of Ta is given in terms of 1000 ppm wt.

nm in diameter. When studied with transmission electron microscopy, the individual grains show a high density of defects, consisting of dislocations and point defect agglomerates (52). The distance between two defects varies from 2 to 20 nm. The onset T_c of as-deposited films is 9.6 K, but the transition width is larger than for bulk niobium (typically a few tenths of a kelvin). The large transition width (5 K in some cases) is indicative of poor film quality.

Although Q_0 values $\approx 10^{10}$ are obtained at low fields, the RF losses of Nb/Cu cavities increase steadily with field. This effect is attributed to intergrain losses in the niobium films, which become more severe at higher frequency. Recently (53), there is evidence to show that impurities buried in the films can also account for increased losses at high fields.

Future Directions, New Materials

Based on the fundamental aspects, for a material to be useful in accelerators, the primary requirements are a high transition temperature and a high superheating critical magnetic field. Among the elemental superconductors, niobium has the highest T_c. While lead, coated on to a copper cavity, has been very useful in early studies and heavy-ion accelerator applications, the higher T_c and H_c has made niobium the more attractive choice. Technical considerations, such as ease of fabrication and the ability to achieve uniformly good material properties over a large surface area, have also proven favorable for niobium. The realm of superconducting compounds has been much less explored because of technical complexities that govern compound formation. In looking at candidates, such as Nb_3Sn, NbN, and the new high-temperature superconductors (HTS), such as $YBa_2Cu_3O_7$, it is important to select a material for which the desired compound phase is stable over a broad composition range. With this criterion, formation of the compound may prove more tolerant to variations in experimental conditions, which in turn would make it possible to achieve the desired single phase over a large surface area. With a T_c of 18 K, Nb_3Sn is the most successful compound explored to date (54). At low fields, residual resistance values comparable to niobium have been achieved. However, the maximum fields reached to date are far lower than those for sheet niobium cavities. The new HTS are even further from the performance level desired for application to accelerators. Figure 14 compares the measured RF surface resistance at low fields of several superconductors: HTS, Nb_3Sn, and Nb (55). The surface resistance of Nb at 1.3 K, Nb_3Sn at 4.2 K, and copper at 77 K are included for comparison.

Early enthusiasm over the remarkable strides made in the transition temperature of HTS are now tempered with difficulties in achieving useful properties, such as a high critical current density. The coherence lengths of the cuprates are very short (17 Å within the copper–oxygen planes and 3 Å perpendicular to the planes, respectively). There is also a large anisotropy of the magnetic and electrical properties between the *c* axis and the *ab* planes, with superior behavior when the current flow is in the *ab* plane. To produce good-quality HTS films, it is therefore necessary to orient the grains so that the *c* axis is normal to the RF surface everywhere. This restriction will be a significant challenge for realizing HTS in existing accelerating cavity shapes. It is also essential to have the right stoichiometry and oxygen content. Because of the short coherence length, transport properties

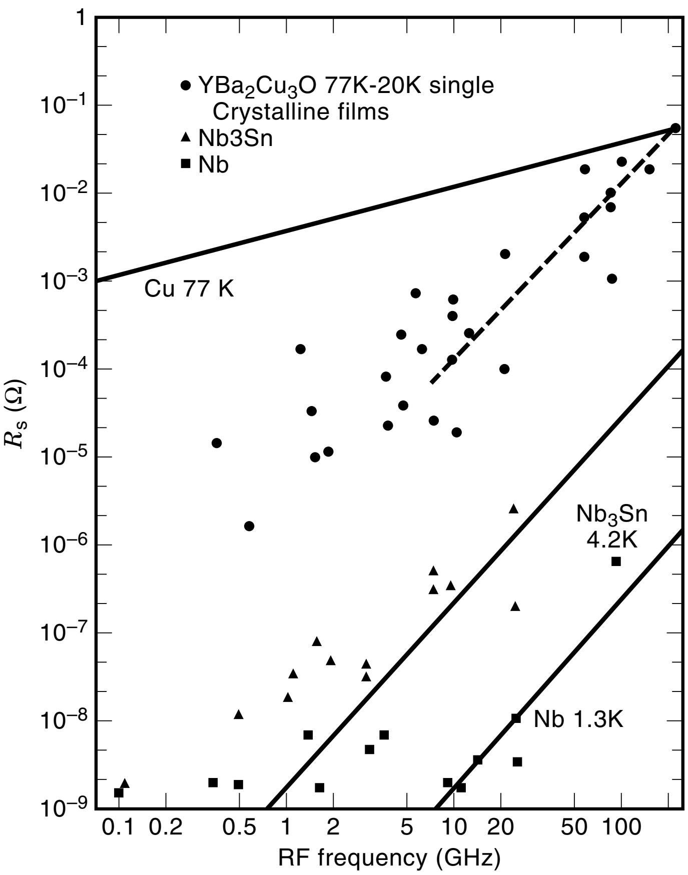

Figure 14. Measured surface resistance of HTS compared to the same for Nb (1.3 K) and Nb_3Sn (4.2 K). In the case of HTS the resistance is quoted at 77 K if it is already residual; if the resistance is still decreasing with temperature, the residual is obtained at 20 K. The solid lines show the calculated surface resistance of copper at 77 K, Nb_3Sn at 4.2 K and Nb at 1.3 K.

are extremely sensitive to minute defects, such as grain boundaries and their associated imperfections. Decoupling of superconducting grains is believed to occur because the coherence lengths approach the scale of the grain boundary thickness, forming only weak links between individual grains. As a result, the intergrain critical current is two to three orders of magnitude lower than intragrain critical current. Even at a clean grain boundary, the scale of the disorder that exists from breaking up of a unit cell can exceed the coherence length, especially in the direction of the *c* axis (56).

CONCLUSION

Even at the modest fraction of the ultimate potential, many attractive applications are now in place, and new ones are forthcoming. As our understanding of field limiting mechanisms continues to improve, new techniques emerge to further advance gradients, such as high-purity niobium to raise the thermal conductivity, high-pressure rinsing to provide cleaner, field emission free surfaces, and high pulsed power processing to destroy residual emitters. The new techniques for bulk niobium cavities have demonstrated that gradients can be improved to between 20 and 30 MV/m in multicell structures. If such gradients can be reliably achieved, exciting new applications are on the horizon, such as the TeV electron–positron linear collider (57) or a multi-TeV muon collider (58).

BIBLIOGRAPHY

1. J. Preble, in B. Bonin (ed.), *Proc. 7th Workshop RF Supercond.,* Gif-sur-Yvette, France, CEA/Saclay 96 080/1, 1995, p. 173.
2. G. Geschonke, in B. Bonin (ed.), *Proc. 7th Workshop RF Supercond.,* Gif-sur-Yvette, France, CEA/Saclay 96 080/1, 1995, p. 143.
3. L. M. Bollinger, *Annu. Rev. Nucl. Particle Sci.,* **36**: 475, 1987.
4. R. Sundelin, *IEEE Trans. Nucl. Sci.,* **NS-32**: 3570, 1985.
5. S. Takeuchi, in K. W. Shepard (ed.), *Proc. 3rd Workshop RF Supercond.,* Argonne National Laboratory, Argonne, IL, ANL-PHY-88-1, 1988, p. 429.
6. H. Padamsee, K. Shepard, and R. Sundelin, *Annu. Rev. Nucl. Particle Sci.,* **43**: 635, 1993.
7. V. L. Ginsburg and L. D. Landau, *Zh. Eksperim. i. Theor. Fizike,* **20**: 1064, 1950.
8. U. Klein and D. Proch, in J. S. McCarthy and R. R. Whitney (eds.), *Proc. Conf. Future Possibilities Electron Accelerators,* Charlottesville, University of Virginia, P. N1-17, 1979.
9. P. Kneisel, R. Vincon, and J. Halbritter, *Nucl. Instrum. Meth.,* **188**: 669, 1981.
10. D. Moffat, in Y. Kojima (ed.), *Proc. 4th Workshop RF Supercond.,* KEK, Tsukuba, Japan, Rep. 89-21, 1990, p. 445.
11. J. Delayen and K. W. Shepard, *Appl. Phys. Lett.,* **57** (5): 514, 1990.
12. H. Padamsee, in *High Voltage Vacuum Insulation,* Latham (ed.), New York: Academic Press, 1995, p. 431.
13. J. Delayen, in Y. Kojima (ed.), *Proceedings of the 4th Workshop on RF Superconductors,* KEK, Tsukuba, Japan, Rep. 89-21, 1990, p. 249.
14. U. Laustroer, U. van Rienen, and T. Wieland, DESY M-87-03, 1988.
15. R. Klatt, DESY M-86-07, 1987.
16. J. Knobloch and H. Muller, *Rev. Sci. Instrum,* **65** (11): 3521, 1994.
17. J. Bardeen, L. N. Cooper, and J. R. Schrieffer, *Phys. Rev.,* **108**: 1175, 1957.
18. D. C. Mattis and J. Bardeen, *Phys. Rev.,* **111**: 412, 1958.
19. J. P. Turneaure, Ph.D. thesis, Stanford University, 1967; see also J. M. Pierce, in L. Marton (ed.), *Methods of Experimental Physics,* Vol. 11, 541, 1974.
20. J. Halbritter, *Z. Physik,* **238**: 466, 1970.
21. See the survey of low field residual resistance values in J. P. Turneaure, *Proc. Appl. Supercond. Conf.,* Annapolis, 1972, p. 621.
22. C. Vallet et al., in E. H. Henke et al. (eds.), *Proc. 1992 European Particle Accelerator Conf.,* Editions Frontieres, 1992, p. 1295.
23. B. Bonin and R. Roeth, in D. Proch (ed.), *Proc. 5th Workshop RF Supercond.,* DESY, Hamburg, Germany, DESY-M-92-01, 1991, p. 210.
24. J. Kirchgessner, in K. W. Shepard (ed.), *Proc. 3rd Workshop RF Supercond.,* Argonne National Laboratory, Argonne, IL, ANL-PHY-88-1, 1988, p. 533.
25. C. Benvenuti, in D. Proch (ed.), *Proc. 5th Workshop RF Supercond.,* DESY, Hamburg, Germany, DESY-M-92-01, 1991, p. 189.
26. Aschroft and Mermin, *Solid State Physics,* W. B. Saunders, 1976, p. 20.
27. L. P. Kadanoff and P. C. Martin, *Phys. Rev.* **124**: 670, 1961.
28. H. Padamsee, J. Knobloch, and T. Hays, *RF Superconductivity for Accelerators,* Wiley, 1998.
29. P. Bernard et al., in H. Henke et al. (eds.), *Proc. 3rd Eur. Particle Accelerator Conf.,* Editions Frontieres, 1992, p. 1269.
30. P. Kneisel, B. Lewis, and L. Turlington, in R. M. Sundelin (ed.), *Proc. 6th Workshop RF Superconductivity,* CEBAF, Newport News, VA, 1994, p. 628.
31. H. Padamsee, J. Tuckmantel, and W. Weingarten, *IEEE Trans. Magn.,* **Mag-19**: 1308, 1983.
32. R. H. Fowler and L. Nordheim, *Proc. R. Soc. London,* **A119**: 173, 1928.
33. J. Knobloch et al., in *Proc. 1995 Particle Accelerator Conf.,* Dallas, 1995, p. 1623.
34. M. Jiminez et al., *J. Phys. D: Appl. Phys.* **27**: 1038, 1994.
35. Q. S. Shu et al., in *IEEE Trans. Magn.* **25**: 1868, 1989.
36. N. S. Xu, in R. V. Latham (ed.), *High Voltage Vacuum Insulation,* Academic Press, 1995, p. 116.
37. W. D. Moeller and M. Pekeler, in S. Myers et al. (ed.), *Proc. 5th European Particle Accelerator Conf.,* Barcelona, Spain, IOPP Publishing, Bristol, 1996, p. 2013.
38. D. Moffat et al., *Particle Accel.,* **40**: 85, 1992.
39. J. Graber et al., *Nucl. Instrum. Meth. Phys. Res.,* **A 350**: 582, 1994.
40. J. Graber et al., *Nucl. Instrum. Meth. Phys. Res.,* **A 350**: 572, 1994.
41. C. Crawford et al., *Particle Accel.,* **49**: 1, 1995.
42. H. Padamsee, *Proc. 1st Workshop RF Supercond.,* KFK, Karlsruhe, Germany, KFK-3019, 1980, p. 145.
43. G. Mueller, in K. W. Shepard (ed.), *Proc. 3rd Workshop RF Supercond.,* Argonne National Laboratories, Argonne, IL, ANL-PHY-88-1, 1988, p. 331.
44. W. Singer, in E. Palmieri (ed.), *Proc. 8th Workshop on RF Supercond.*, Abano Terme, Italy, 1997, in press.
45. K. K. Schulze, *J. Metals,* **33**: 33, 1981.
46. K. Schulze, Niobium, in H. Stuart (ed.), *Proc. Int. Symp.,* San Francisco, The Metallurgical Society of AIME, 1981, p. 163.
47. A. Gladun et al., *J. Low Temp. Phys.,* **27**: 873, 1977.
48. H. Padamsee, in R. M. Sundelin (ed.), *Proc. 6th Workshop RF Supercond.,* CEBAF, Newport News, VA, 1994, p. 515.
49. A. V. Elyutin, et al., in D. Proch (ed.), *Proc. 5th Workshop RF Supercond.,* DESY, Hamburg, Germany, DESY-M-92-01, 1991, pp. 354, 426.
50. H. Padamsee, in H. Lengeler (ed.), *Proc. 2nd Workshop RF Supercond.,* CERN, Geneva, Switzerland, CERN, 1984, p. 339.
51. P. Kneisel, *J. Less Common Metals,* **139**: 179, 1988.
52. C. Durand and W. Weingarten, *IEEE Trans Appl. Supercond.,* **5**: 1107, 1995.
53. S. Calatroni, in E. Palmieri (ed.), *Proc. 8th Workshop RF Supercond.,* Abano Terme, Italy, 1997, in press.
54. M. Peiniger, in K. W. Shepard (ed.), *Proc. 3rd Workshop RF Supercond.,* Argonne National Laboratory, Argonne, IL, ANL-PHY-88-1, 1988, p. 503.
55. D. Busch et al., in R. M. Sundelin (ed.), *Proc. 6th Workshop RF Supercond.,* CEBAF, Newport News, VA, 1994, p. 173.
56. G. Mueller, in Y. Kojima (ed.), *Proc. 4th Workshop RF Supercond.,* KEK, Tsukuba, Japan, Rep. 89-21, 1990, p. 267.
57. R. Brinkmann, in *Proceedings of the 1995 Particle Accelerator Conference,* Cat. No. 95CH35843, 1995, p. 674.
58. $\mu^+\mu^-$ *Collider, A Feasibility Study,* BNL-52503, 1996.
59. P. Wilson, in R. A. Carrigan, F. R. Huson, and M. Month (eds.), *Physics of High Energy Particle Accelerators (Fermlab Summer School, 1981),* AIP Conf. Proc., no. 87, American Institute of Physics, 1982.

HASAN PADAMSEE
Cornell University

SUPERCONDUCTING COILS. See SUPERCONDUCTING MAGNETS, QUENCH PROTECTION.